INTERNATIONAL JOURNAL OF
NUMERICAL ANALYSIS AND MODELING, Series B
Volume 3, Number 1, Pages 20–35

BRAIN DEFORMATION UNDER MILD IMPACT: MAGNETIC RESONANCE IMAGING-BASED ASSESSMENT AND FINITE ELEMENT STUDY

YING CHEN, BRAD SUTTON, CHARLES CONWAY, STEVEN P. BROGLIO,
AND MARTIN OSTOJA-STARZEWSKI

Abstract. The knowledge of in vivo human brain deformation within the skull is essential in understanding brain injury mechanisms. Such measurements have become possible only in recent years thanks to the advancement of magnetic resonance imaging (MRI) technique. In this paper, we first study in vivo human brain deformation under mild impact induced by a 2-cm head drop using tagged MRI and the harmonic phase (HARP) imaging analysis technique originally developed for cardiac motion analysis. A finite element (FE) simulation of mild impact is then carried out using a patient-specific 3-D head model. A reasonably good correlation is found between the predicted deformation field from FE modelling and the results from MRI-based assessment. It is found that the maximum deformations occur within a few milliseconds following the impact, which is during the first oscillation of the brain within the skull, with the maximum displacements of 2-3 mm and the maximum strains of 5-10%. To our knowledge, this study is the first attempt where the deformation field obtained by MRI-based assessment is correlated with the prediction of a corresponding FE model, and it is also the first validation of a FE brain injury model on in vivo human brain deformation data.

Key words. brain injury; magnetic resonance imaging; image processing; finite element modelling

1. Introduction

To gain understanding of brain injury mechanisms, researchers have long been interested in brain deformation within the skull under various traumatic loading conditions. However, direct observation of human brain deformation in vivo is extremely difficult. Therefore, physical models such as animals, human cadavers, and inanimate replicas have been used in the past to study deformation patterns of the brain under either impact or impulsive loading. To track brain motion, different techniques utilized in physical experiments include high speed X-ray with embedded radioactive markers in test animals or human cadavers [7, 8, 12, 17], use of Lucite calvarium to replace a portion of the skull for direct observations of brain motion [5, 15], and use of gelatin models to simulate brain material [6, 9, 11]. The experimental studies using above techniques have contributed significantly to our understanding of brain injury mechanisms in the past several decades. However, the extent to which the experimental results may be applied to human brain in vivo is uncertain due to the discrepancies of geometry and material properties between in vivo human brain and each of these physical models. To obtain a better understanding of brain injury mechanisms, the use of in vivo human brain for experimental studies plays an irreplaceable role, and such experiments have become possible since the invention and advancement of the medical imaging technique, the magnetic resonance imaging (MRI).

MRI is known to be the most powerful tool for non-invasive assessment of biological soft tissues in vivo, which makes it suitable for brain research. In fact, in

Received by the editors August 17, 2011.
2000 *Mathematics Subject Classification.* 74Hxx, 74M20, 74S05, 92C55, 94A08, 94A12.

the field of cardiac research, a special MRI pulse sequence called tagging [1, 18] has been developed and has become a well established technique to image cardiac motion. MRI tagging is used to spatially modulate the longitudinal magnetization of the subject to create temporary features called tags in the myocardium. The tag pattern is subsequently deformed by the heart motion and can be visualized in an image sequence reconstructed from sufficient data acquired over many heartbeats in a single breath hold [14]. Various image processing techniques have also been developed to analyze the tagged cardiac MRI images to estimate the motion quantities such as displacements and strains of the myocardium. In particular, a novel image processing technique called harmonic phase (HARP) image analysis developed in [13, 14] provides a fast and automated means to estimate dense motion quantities from tagged cardiac MRI images. The tagged MRI and the HARP image processing techniques developed for cardiac motion tracking has been applied to obtain deformation fields of in vivo human brain during mild acceleration [2, 4, 16].

Our present study not only deals with kinematics of a deforming brain which is motivated by Bayly et al.'s work [2], but also includes a mechanical model that deals with the mechanics from the standpoint of Newtonian dynamics, i.e. also including momentum balances and constitutive laws. In this paper, we study the brain deformation induced in mild impact from a 2 cm vertical head drop. We carry out the head drop experiments using human volunteers, acquire tagged MRI images during the head drop, apply the HARP analysis to the tagged MRI images, and obtain the brain motion estimates. In addition, we build a mathematical model of mild impact of the human head through finite element (FE) modelling, and compare the predicted deformation fields with those from MRI-based HARP estimates. The significance of the comparison is two-fold. On one hand, to the best of our knowledge, this is the first attempt where the deformation field obtained by MRI-based assessment (i.e., tagged MRI images and HARP analysis) is correlated with predictions of a corresponding FE model. A good correlation provides a validation of the sensitivity of the tagged MRI and HARP analysis to the deformations caused by the mild impact loading. On the other hand, our work is also the first attempt to use deformations of in vivo human brain for FE head injury model validation. A good correlation serves as a validation of our proposed FE model for brain injury research.

2. Methods

The organization of this section is as follows. First, we present our head drop experiment, tagged MRI image acquisition, and the implementation of the HARP image processing technique to track brain motion induced in mild impact. Secondly, the FE modelling of mild impact is described.

2.1. MRI-based assessment of brain deformation. A healthy adult with no history of head trauma was recruited to participate in the 2-cm vertical head drop experiment. The experiment was carried out at the Biomedical Imaging Center (BIC) at the University of Illinois at Urbana-Champaign in accordance with the Institutional Review Board. All MRI data collection was performed on a Siemens Allegra 3T scanner. During the 2 cm vertical head drop, a custom-made MRI-compatible head drop device (HDD) is secured to the MRI head coil to guide the motion of head (Fig. 1), and the occipital region of the head is impacted with a rigid plate after the drop. At the start position, the HDD is raised to the elevated position and locked. As the head begins to drop after activation of a release mechanism, a fiber optic system of the HDD triggers the dynamic imaging sequence of the MRI

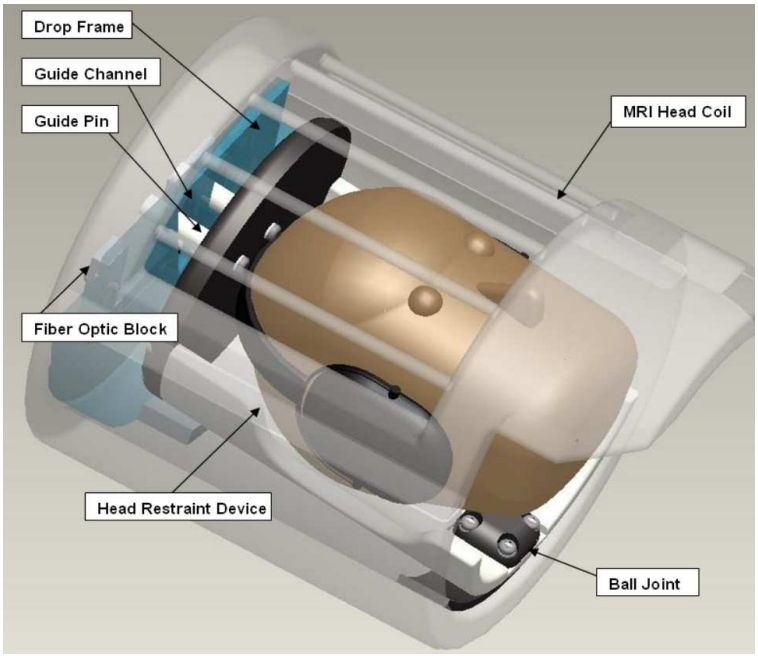

FIGURE 1. HDD complete unit CAD model.

unit. The dynamic scans utilize a multi-shot spiral FLASH sequence with spatial modulation of magnetization (SPAMM) grid-tagging and the grid-tagging lines are applied in synchrony with the head drop. The imaging sequence parameters are: TR=10 ms, TE=1.5 ms, flip angle=8°, 240 mm field of view, 128×128 acquisition matrix, 1.8 mm spatial resolution, 10 ms temporal resolution, 4 mm tag period, and 8 mm slice thickness. A 12-shot spiral acquisition is used, where a single shot at each time point is acquired per head drop and the drop is repeated 12 times per image time series. Four series of dynamic images are acquired. They include one axial slice and one sagittal slice, and two tagging orientation per image slice. Slice prescription is determined by examining the lowest point of the skull in a scout image taken with the HDD in the down position. 200 tagged images are acquired in a time series, covering the first two seconds after the head drop with 10 ms temporal resolution. Figure 2 shows the SPAMM-tagged images corresponding to the 7th time point (70 ms) after the drop.

The HARP method is based on the fact that the spatial modulation of magnetization (SPAMM)–tagged MRI images [1] have a collection of distinct spectral peaks in the Fourier domain, and each of these spectral peaks carries information about a particular component of tissue motion. The inverse Fourier transform of one of these peaks is a complex image called the harmonic image. It can be shown that the phase of the harmonic image is linearly related to a directional component of the tissue motion and this phase-motion relation is the key to the ability

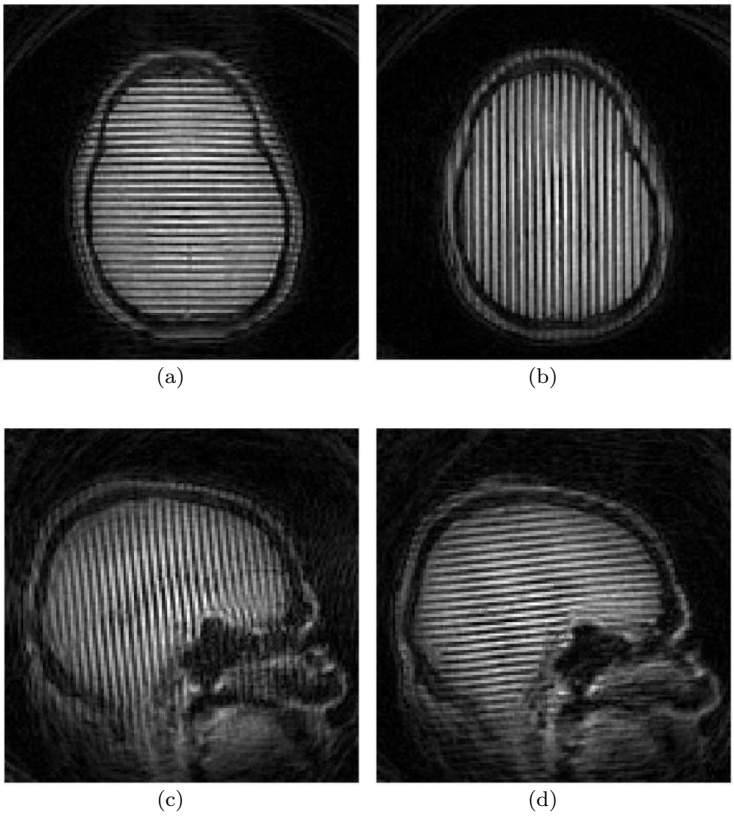

FIGURE 2. MRI SPAMM-tagged images corresponding to 70 ms after tagging. (a) Anterior-posterior SPAMM tags and (b) left-right SPAMM tags in the axial slice. (c) Anterior-posterior SPAMM tags and (d) head-feet SPAMM tags in the sagittal slice.

of the HARP method to track motion with sub-voxel resolutions. The summary of the methodology of the HARP image processing technique developed by Osman et al. [13, 14] and the implementation details of our brain motion estimates are given in the Appendix. The implementation of the HARP method for displacement estimates using tagged MRI images include the following four major steps: obtain Fourier transform SPAMM-tagged images to get isolated spectral peaks; apply a band-pass filter to isolate one of the off-center harmonic peaks; take Fourier transform of the isolated peak to get a harmonic image; obtain the HARP angle image which is the principal value of the phase of the harmonic image; use the HARP angle images to estimate the two-dimensional (2-D) displacement fields.

As an example, Fig. 3(a) shows the spectral peaks for the tagged image in Fig. 2(a). Figure 3(b) shows the harmonic magnitude image extracted from the tagged image shown in Fig. 2(a) using the filter in Fig. 3(a). The HARP angle image corresponding to the spectral peak circled in Fig. 3(a) is shown in Fig. 3(c), and a mask created using a crude segmentation of the harmonic magnitude image in Fig. 3(b) is applied to remove noise outside the region of interest.

A custom MATLAB code has been developed for implementing the HARP method for estimating the motion. Given four series of SPAMM-tagged images

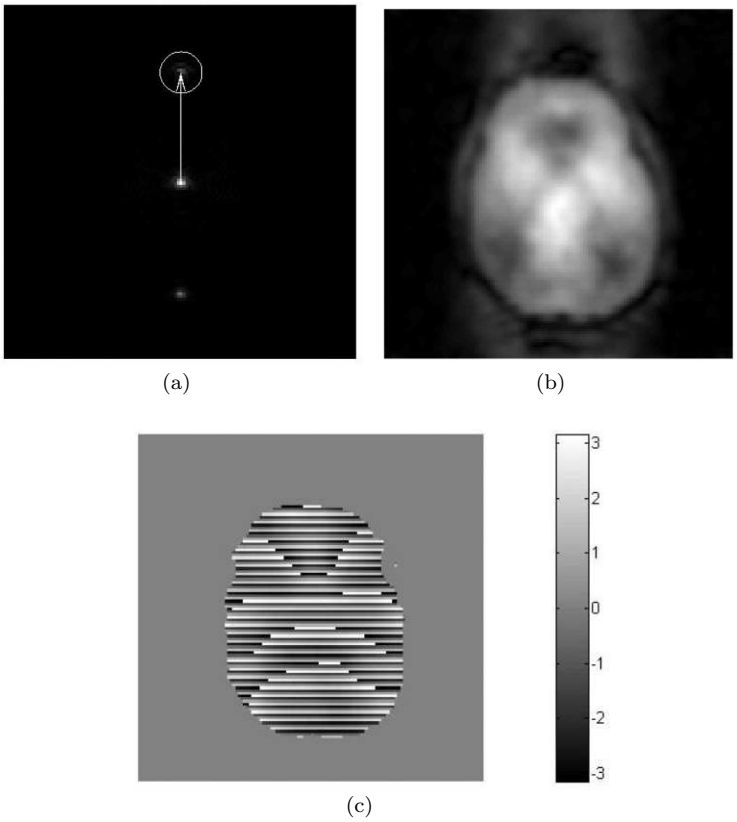

(a) (b)

(c)

FIGURE 3. (a) Magnitude of Fourier transform of Fig. 2(a). (b) Harmonic magnitude image of a harmonic image corresponding to the spectral peak inside the circle in (a). (c) Harmonic phase angle image of the harmonic image corresponding to the same spectral peak as in (b).

described earlier in MRI data collection, a sequence of 2-D displacement fields for both axial slice and sagittal slice are obtained. In a preliminary study, we obtained displacements at each time point relative to the previous time point. For example, the displacement at 70 ms is the displacement of 70 ms relative to 60 ms. From such a sequence of relative displacements, we find that the brain experiences downward displacements in the direction of the impact for each time instant during the first 60 ms, which is the free fall period of a 2 cm vertical drop. At 70 ms, the brain starts to have upward displacement, which indicates it has begun to bounce from the impact. This observation seems reasonable since a particle dynamics analysis shows it takes about 63 ms for a rigid body to impact with a rigid surface after a 2 cm drop. The brain continues to move upward at 80 - 100 ms, but the rate of change of displacements slows and stops. After 100 ms, the brain falls back down until it hits the lowest position at around 140 ms. After 140 ms, the upward displacements of the brain resume, indicating the start of the second oscillation, which ends around 200 ms when the brain hits the lowest position again. Then a few more small oscillations follow before the brain motion diminishes. Since the brain motion after impact is of our primary interest, we safely assume 60 ms is

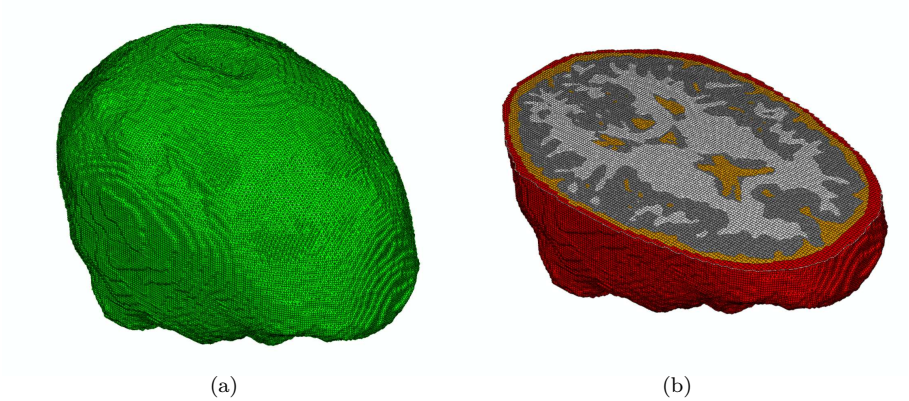

(a) (b)

FIGURE 4. (a) FE model of the human head; (b) FE model of the human head – axial view.

the instant right before impact, based on the above analysis, and recalculate the displacements using the time frame at 60 ms as our reference time frame.

2.2. FE simulation of mild impact. Our previously developed patient-specific MRI voxel-based FE mesh of the human head [3] is used in this study. The geometry of the FE mesh is based on T1- and T2-weighted structural MRI scan data of a healthy adult. Image segmentation is performed using FMRIB Software Library (FSL) to differentiate five tissue types: scalp, skull, cerebrospinal fluid (CSF), gray matter, and white matter. As a result, each image voxel is associated with a particular tissue type. The FE mesh shown in Fig. 4 is created by directly converting image voxels into eight-node hexahedral elements through a custom C++ code. The FE mesh consists entirely of hexahedral elements with element size of which is identical to the MRI resolution. Each FE is assigned a particular material property according to the tissue type of its corresponding image voxel. The scalp and facial structures are excluded, and structures such as membranes and blood vessels are not explicitly modeled. Globally, the model has a total of 1,061,799 elements and 1,101,599 nodes. In order to improve numerical accuracy, a mesh smoothing technique is also applied to smooth out the jagged edges on the outer surface and material interfaces. The details of the mesh generation and mesh smoothing algorithm are described in [3]. To the best of our knowledge, our MRI voxel-based FE head model was the first FE head model that has the MRI resolution. The voxel-based mesh generation method provides an efficient and accurate means of generating a patient-specific head mesh that can describe the important features of the highly complex head geometry, such as the folding structure of the cerebral cortex and realistic separation of CSF, gray, and white matter. The very fine mesh of our model also makes it possible to capture stress wave propagation during a head impact process as demonstrated in our previous study [3].

The material data of different tissues used in this study are taken from literature [10, 19] and listed in Table 1. The CSF is modeled using solid FEs to account for the shear resistance provided by the arachnoid trabeculae and large blood vessels in the subarachnoid space. All material phases in the model are assumed to be homogeneous and isotropic. While the skull and CSF are assumed to be linear elastic, the brain tissues are taken as linear viscoelastic in shear but elastic in bulk

behavior. The shear relaxation modulus is described by

$$G(t) = G_\infty + (G_0 - G_\infty)e^{-\beta t} \tag{1}$$

where G_0 is the short-term shear modulus, G_∞ is the long-term shear modulus, and β is the decay constant.

TABLE 1. Mechanical properties of different tissues used in the FE model

Tissue	Density ρ (kg/m^3)	Bulk modulus K (Pa)	Short term modulus G_0 (Pa)	Long term modulus G_∞ (Pa)	Decay factor β (sec^{-1})
Skull	2070	$3.61E+9$	$2.7E+9$	$2.7E+9$	N/A
CSF	1004	$2.19E+7$	$5.0E+4$	$5.0E+4$	N/A
Grey matter	1040	$2.19E+9$	$3.4E+4$	$6.4E+3$	400
White matter	1040	$2.19E+9$	$4.1E+4$	$7.8E+3$	400

Traction and displacement continuity at material interfaces are assumed in the FE model, in such a way that neither tangential sliding nor normal separation is allowed at any two-tissue interface. The interface condition can be described mathematically as follows:

$$\left.\begin{array}{l} \mathbf{u}^{(p)} = \mathbf{u}^{(q)} \\ \mathbf{t}^{(p)} = \mathbf{t}^{(q)} \end{array}\right\} \text{ for all } p \text{ and } q \text{ phases in contact,} \tag{1}$$

where $\mathbf{u}$ is the displacement vector and $\mathbf{t}$ is the traction vector. Since the neck is not included in our model, an appropriate boundary condition must be prescribed to simulate the constraint of the neck on the head movement during the head drop. In this study, a fixed boundary condition is prescribed around the region of foramen magnum to represent the restraining effect of the neck.

Besides the head model, a rigid surface that the occipital region of the head will impact is also defined. Since the brain deformation after impact is of more interest than its behavior during the free fall before impact, we model the head at an initial position very close to the rigid surface and specify an initial velocity of 0.626 m/s which is the final velocity of a 2 cm vertical drop based on a particle dynamics analysis. To model the interaction between the human head and the rigid surface, a friction coefficient of 0.3 is specified for tangential behavior. The simulation is then run using ABAQUS with a dynamic, explicit procedure for 150 ms.

3. Results

The 2-D displacement fields obtained by MRI-based HARP analysis for both axial and sagittal slices from 70 ms to 200 ms using 60 ms as the reference time frame are shown in Fig. 5(a), (c) and Fig. 6(a), (c). For the axial slice, the maximum displacements in the anterior-posterior direction reach over 1 mm after impact, whereas the displacement in the left-right direction is not significant throughout the duration. For the sagittal slice, the displacements in the anterior-posterior direction reach between 2 and 3 mm in the top portion of the brain whereas the displacement in the head-feet direction is within 2 mm range. The magnitude of the maximum displacement is consistent with those obtained by Feng et al [4]. Comparing the displacement fields between the first oscillation of the brain (70 ms - 140 ms) and the second oscillation (150 ms - 200 ms) for all cases, we see that a larger portion of the brain experiences large displacements during the first oscillation. Notice that the anterior-posterior displacements in the sagittal slice (Fig. 6(a)) is vertically

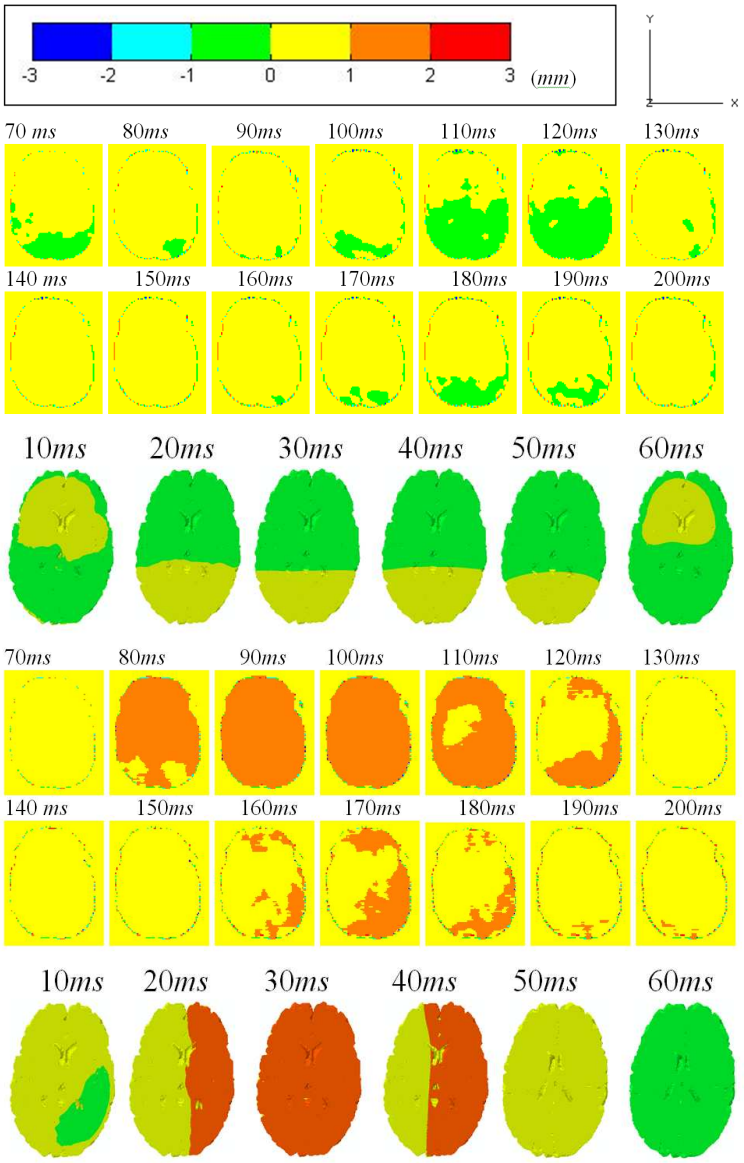

FIGURE 5. In-plane displacement fields for the axial plane obtained from HARP analysis and FE simulation.

varied, and the top portion of brain tissues has larger displacements than the lower portion. This pattern is understandable since the lower portion of the brain, the brain stem, extends to the neck which provides some degree of constraint to the movement around that region. Another reason can be that the base of the skull is very rough while the top of the skull is relatively smooth, so lower portion of the brain cannot move much compared to its upper portion.

The axial and sagittal planes in the FE model that are close to the slice prescription in the MRI data collection are determined. The in-plane displacement fields obtained by FE simulation for the first 60 ms with 10-ms interval are shown

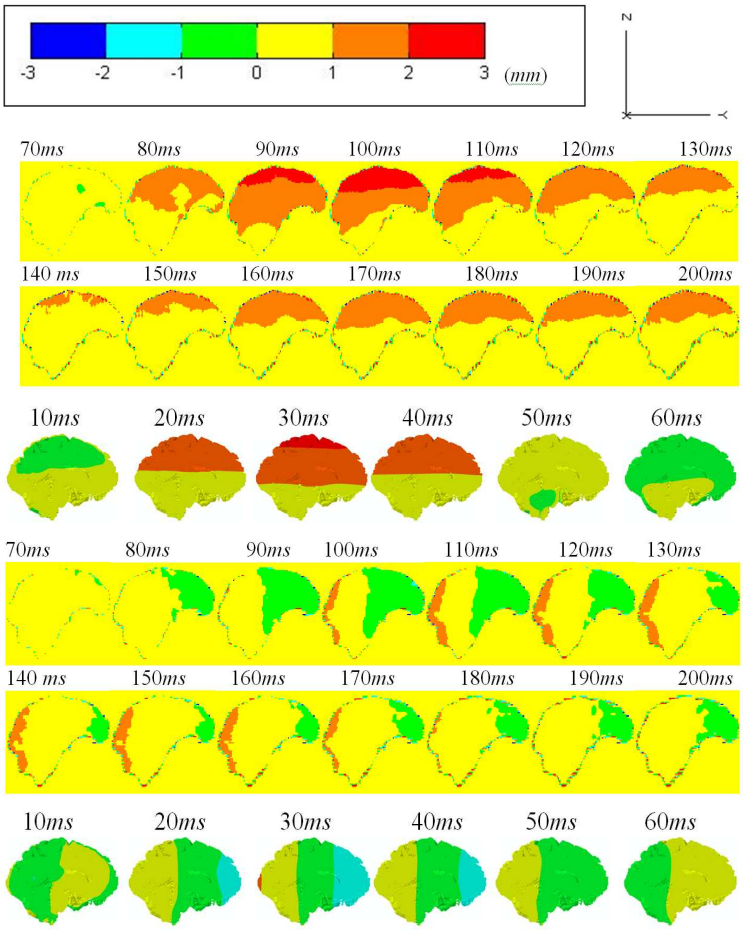

FIGURE 6. In-plane displacement fields for the sagittal plane obtained from HARP analysis and FE simulation.

in Fig. 5(b), (d) and in Fig. 6 (b), (d) for comparison with the results from MRI image-based HARP analysis. We find that, at 5 ms, the displacements (not shown in Figs. 5 and 6) in the direction of the impact in both the axial and sagittal slice are negative. This initial downward displacement is due to the fact that the head model is placed initially at a position above the rigid surface. However, at 10 ms we start to see upward displacements. Therefore, we consider the time frame at 10 ms in the FE simulation to correspond approximately to the time frame at 70 ms in the HARP analysis, but note that the reference position in the FE simulation is not exactly the same as the reference position in the HARP displacement estimates. This discrepancy can be one of the reasons for possible differences in results obtained through these two different methods.

The magnitude of the maximum displacement predicted by the FE simulation is on the same order as that obtained by the HARP analysis, i.e., in the range of 1-2 mm for the axial slice and 2-3 mm for the sagittal slice. For the sagittal slice, the patterns of displacement distribution from the HARP analysis are also predicted by the FE simulation, which involve vertically varying displacements in

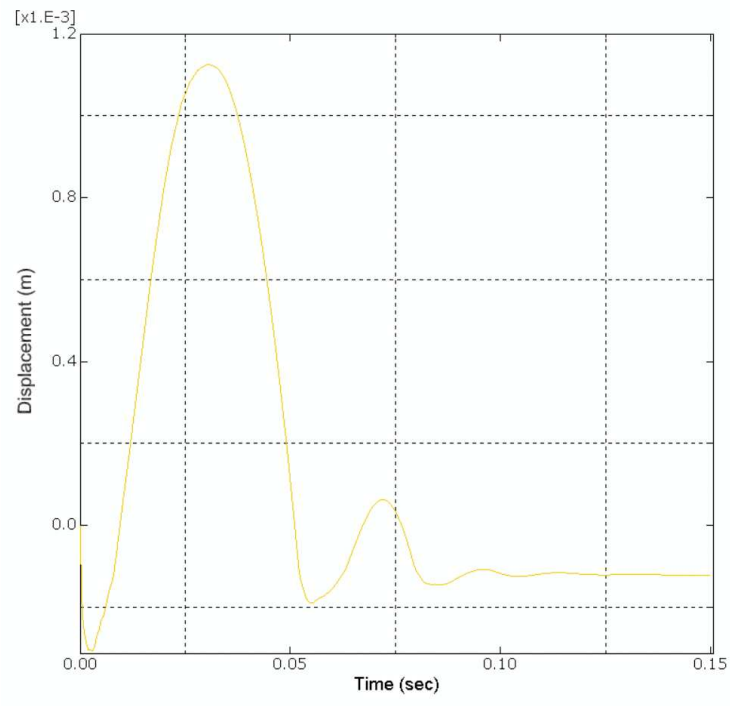

FIGURE 7. Displacement time history of a node on the brain close to the impact site obtained from FE simulation.

the anterior-posterior direction and horizontally varying displacements in the head-to-feet direction. One may also notice the displacements in the anterior-posterior direction for the axial slice as shown in Fig. 5(d) are not perfectly symmetric about the midline. The asymmetric displacements may be caused by an imperfectly symmetric brain dropping at a slightly tilted angle.

Differences in the displacement fields obtained from these two methods are also observed. First, the duration of the first oscillation of the brain in FE simulation is about 60 ms, which is less than that in the HARP analysis (˜80 ms). Figure 7 shows the predicted displacement time history of a node in the occipital region of the brain that is close to the impact region. The period of the first oscillation of the FE model can be attenuated by changing the prescribed fixed boundary condition around foramen magnum.

A more compliant boundary condition would result in a longer period of the first oscillation. Second, the displacement pattern in left-right direction in the axial slice (Fig. 5(a) and (b)) obtained from these two methods seems to be reversed. In the HARP analysis, displacement is positive in the anterior portion and negative in the posterior portion for most of the duration. The FE simulation gives just the opposite results. While this discrepancy in lateral displacements is small in magnitude, and therefore of secondary importance, the reason for it to occur is not clear. Third, the negative displacements seen at 10 ms and 60 ms in the axial slice (Fig. 5(d)) do not appear in the displacement estimates by HARP analysis. This difference can be attributed to different reference positions for displacement calculations. Fourth, in the sagittal slice, the FE simulation predicts the switch of signs of displacements at the beginning of the second oscillation (from 50 ms to 60

ms as shown in Fig. 6(b) and (d)) which is not seen in the results obtained by the HARP analysis.

Given the significant complexity of the head motion and brain deformation under mild impact, we have obtained a reasonably good correlation of the in-plane brain displacements with the prediction of the FE model and the estimates of the MRI-based HARP analysis, especially during the first oscillation of the brain within the skull.

4. Discussion and Conclusions

In vivo human brain deformation has been studied through MRI-based assessment by [2, 4]. One drawback in these studies is that a large number of repeated drops (the total of 288 drops per study) are required. The acquisition of 72 drops per image sequence is required in order to get good spatial and temporal resolution in the resulting dynamic images. Slight changes in the performance of the drop over time will result in errors. These changes in performance include timing, anticipation of the subject, and impact angle as the head shifts in the dropping frame. Additionally, two image slices (axial and sagittal) and two tagging orientations per image slice needed to track brain motion result in $4 \times 72 = 288$ drops per subject [2], which is prohibitive in terms of repeatability and in subject compliance. In the curren study, our implementation takes advantage of dynamic MRI imaging methodology using spiral trajectories and therefore requires fewer head drops in order to compose a time series. We have used a multi-shot spiral acquisition and require only 12 drops per image, a reduction in drops by a factor of 6. The experiment requires a total of 48 drops per study, which improves both the quality of the data and the experience of the subject, making the analysis suitable to a wider population.

Besides displacements, strain fields are also obtained by FE simulation, which provides a better measure of brain deformation. Brain tissue is most vulnerable to shear strains due to its high bulk modulus and low shear modulus. In addition, tensile strains are believed to be more dangerous than compressive strains. Here we show the in-plane shear strain and the maximum principal strain distribution in the prescribed axial and sagittal slice for the first 60 ms after impact with 5-ms interval in Figs. 8 and 9, respectively. For the axial slice, the maximum shear strains are within 3% and the maximum principal strains are within 5%. Larger shear strains and maximum principal strains are seen in the sagittal slice, which are more than 5% but within 10%. In both the axial and sagittal slices, we see the maximum strains to occur in the first few milliseconds after impact, which is during the first oscillation of the brain within the skull. Under moderate or severe impact, we would expect the brain to experience strains larger than 10% during the initial time following the impact, which can be the cause of immediate functional or structural damage to brain tissues.

A few limitations of current study should be noted. First, only in-plane displacement fields of the prescribed axial and sagittal slices are obtained through MRI-based HARP analysis due to the limitation of current MRI tagging technique. Once 3-D tagged image data becomes available, a full comparison of 3-D spatio-temporal displacement fields can be made with the results from FE modelling. Second, the mild impact considered in this study is well under brain injury threshold and high strength impact can only be studied using physical models such as human cadavers and animal models. However, our study of mild impact can provide some insight into the deformation patterns of the brain under more severe impact.

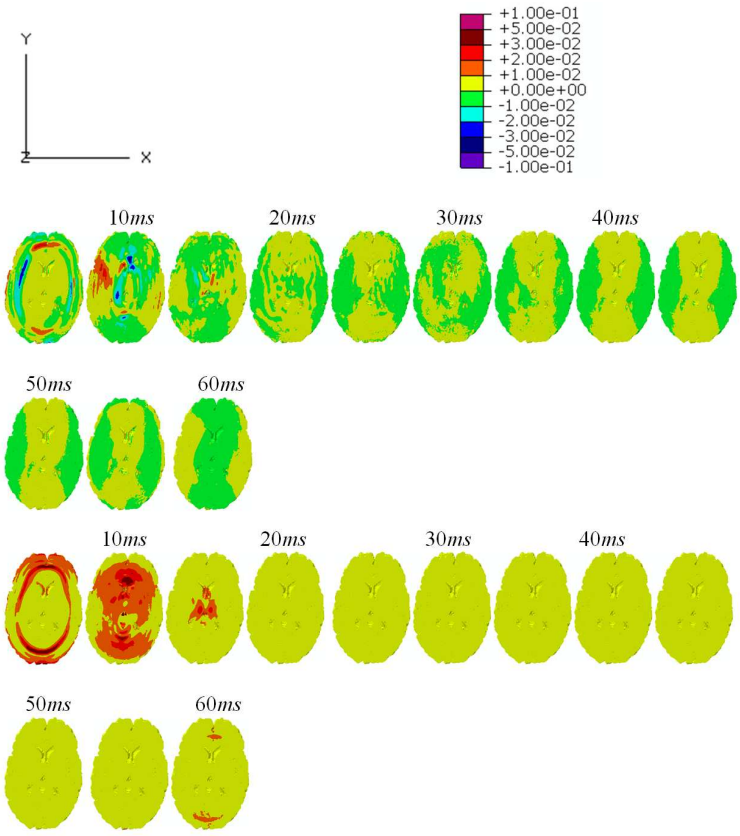

FIGURE 8. In-plane shear strains and maximum principal strains for the axial slice predicted by FE simulation.

In summary, deformation patterns of human brain under mild impact are studied through two different methods: MRI-based assessment of in vivo human brain and FE modelling. The 2 cm vertical head drop experiments were carried out in the MRI tunnel to induce mild impact to the human head. Tagged MRI images were acquired and HARP image processing technique was implemented to obtain displacement fields of the brain under mild impact. A 3-D FE head model was constructed and the simulation of the mild impact event was carried out to predict the spatio-temporal distribution of deformation fields including displacements and strains of the brain. A reasonably good correlation was found between the displacement fields obtained through MRI-based HARP analysis and through the FE simulation. To the best our knowledge, our study is the first validation of an FE brain injury model on in vivo brain deformation data, and it is also the first attempt where the deformation field obtained by tagged MRI and HARP image processing technique is correlated with predictions of a corresponding FE model.

From an engineering point of view, the final objective of brain injury research is to provide a predictive tool such as an FE model that can aid in injury diagnosis and design of protective devices. A well validated FE model can be such a powerful tool, especially when brain injury experiments are difficult and expensive to carry out. Our previously proposed 3-D MRI-based patient-specific FE head model

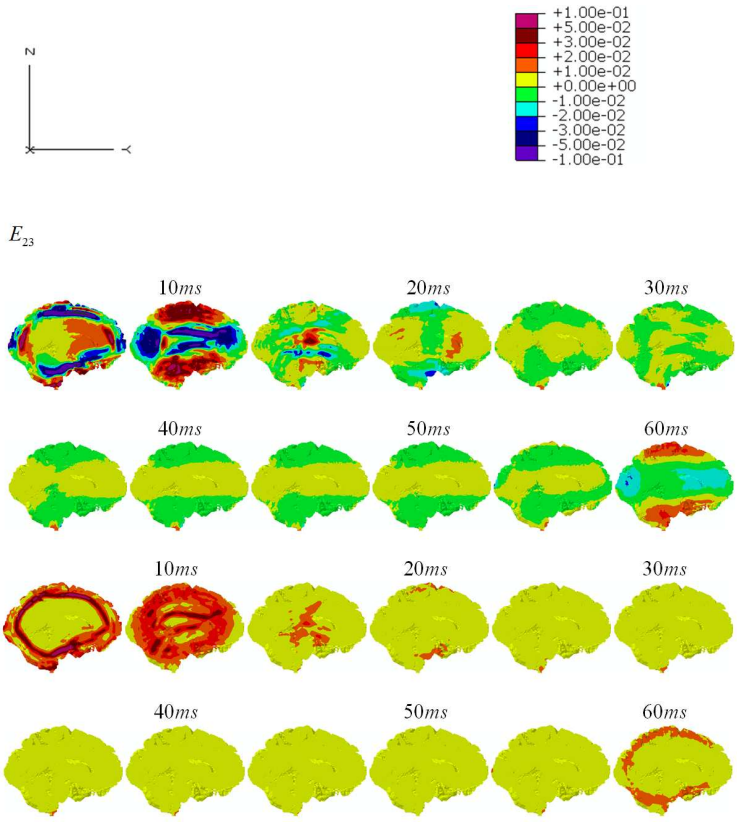

FIGURE 9. In-plane shear strains and maximum principal strains for the sagittal slice predicted by FE simulation.

has been validated using intracranial pressure data of human cadavers subject to frontal impact [3]. While we are making ongoing improvements of our FE model by adding structures such as membranes and blood vessels, as well as adopting more sophisticated material models and interface/boundary conditions, the new validation using in vivo brain deformation data under mild impact in this study provides us more confidence of using our proposed FE model as an effective predictive tool for future brain injury research.

Acknowledgments

This work was partially supported by the Beckman Institute at the University of Illinois and the NSF under the grant CMMI-1030940.

References

[1] L. Axel, and L. Dougherty, MR imaging of motion with spatial modulation of magnetization, *Radiology*, 171: 841-845 (1989).

[2] P.V. Bayly, T.S. Cohen, E.P. Leister, D. Ajo, E.C. Leuthardt, and G.M. Genin, Deformation of the human brain induced by mild acceleration, *J. Neurotrauma*, 22: 845-856 (2005).

[3] Y. Chen, and M. Ostoja-Starzewski, MRI-based finite element modeling of head trauma: spherically focusing shear waves, *Acta Mechanica*, 213: 155-167 (2010).

[4] Y. Feng, T.M. Abney, R.J. Okamoto, R.B. Pless, G.M. Genin, and P.V. Bayly, Relative brain displacement and deformation during constrained mild frontal head impact, *Journal of Royal Society Interface*, 7: 1677-1688 (2010).

[5] H.H. Gosch, E. Gooding, and R.C. Schneider, The Lexan calvarium for the study of cerebral responses to acute trauma, *J. Trauma*, 10: 370-376 (1970).
[6] E.S. Gurdjian, and H.R. Lissner, Photoelastic confirmation of the presence of shear strains at the craniospinal junction in closed head injury, *J. Neurosurg.*, 18: 58-60 (1961).
[7] W.N. Hardy, C.D. Foster, M.J. Mason, K.H. Yang, A.I. King, and S. Tashman, Investigation of head injury mechanisms using neutral density technology and high-speed biplanar X-ray, *Stapp Car Crash J.*, 45: 337-368 (2001).
[8] V.R. Hodgson, E.S. Gurdjian, and L.M. Thomas, Experimental skull deformation and brain displacement demonstrated by flash x-ray technique, *J. Neurosurg.*, 25: 49-52 (1966).
[9] A.H. Holbourn, Mechanics of head injury, *Lancet 2*: 438-441 (1943).
[10] T.B. Khalil, and R.P. Hubbard, Parametric study of head response by finite element modeling, *J. Biomech.*, 10: 119-132 (1977).
[11] S.S. Margulies, L.E. Thibault, and T.A. Gennarelli, Physical model simulations of brain injury in the primate, *J. Biomech.*, 23: 823-836 (1990).
[12] G.S. Nusholtz, P. Lux, P.S. Kaiker, and M.A. Janicki, Head impact response – skull deformation and angular accelerations, In: *Proc. 28th Stapp Car Crash Conf.*, 41-74 (1984).
[13] N.F. Osman, and J.L. Prince, Angle images for measuring heart motion from tagged MRI, In: *Proc. Int. Conf. Imaging Proc.*, 1: 704-708 (1998).
[14] N.F. Osman, E.R. McVeigh, and J.L. Prince, Imaging heart motion using harmonic phase MRI, *IEEE Trans Med Imaging*, 19: 186-202 (2000).
[15] R.H. Pudenz, and C.H. Shelden, The Lucite calvarium – a method for direct observation of the brain. II. Cranial trauma and brain movement, *J. Neurosurg.*, 3: 487-505 (1946).
[16] A.A. Sabet, E. Christoforou, B. Zatlin, G.M. Genin, and P.V. Bayly, Deformation of the human brain induced by mild angular head acceleration, *J. Biomech.*, 41: 307-315 (2008).
[17] S.A. Shatsky, D.E., Evans, F. Miller, and A. Martins, High-speed angiography of experimental head injury, *J. Neurosurg.*, 41: 523-530 (1974).
[18] E.A. Zerhouni, D.M. Parish, W.J. Rogers, A. Yang, and E.P. Shapiro, Human heart: tagging with MR imaging – a method for noninvasive assessment of myocardial motion, *Radiology*, 169: 59-63 (1988).
[19] L. Zhang, K.H. Yang, and A.I. King, A proposed injury threshold for mild traumatic brain injury, *J. Biomech. Eng.*, 126: 226-236 (2004).

5. Appendix: Summary of HARP Image Processing Technique for Displacement Estimates

An image point can be defined by a 2-D vector $\mathbf{y} = [y_1, y_2]^T$, where y_1 is the coordinate in the readout direction and y_2 the coordinate in the phase-encoding direction. In order to relate 2-D tagged images to actual 3-D tissue motion, a fixed rectangular Cartesian coordinate system, $\mathbf{x} \in \mathbb{R}^3$, representing the scanner frame is also defined. The actual 3-D position $\mathbf{x}$ of an image point $\mathbf{y}$ is therefore given by the function

$$\mathbf{x}(\mathbf{y}) = y_1\mathbf{h}_1 + y_2\mathbf{h}_2 + \mathbf{x}_0 = \mathbf{H}\mathbf{y} + \mathbf{x}_0, \tag{A1}$$

where $\mathbf{h}_1 \in \mathbb{R}^3$ and $\mathbf{h}_2 \in \mathbb{R}^3$ are the readout and phase-encoding directions of the image plane, respectively, $\mathbf{H} = [\mathbf{h}_1, \mathbf{h}_2]$, and $\mathbf{x}_0 \in \mathbb{R}^3$ is the origin of the image plane. At time $t = 0$, let every material point be marked by its position $\mathbf{p} \in \mathbb{R}^3$. As the brain tissue deforms, a material point moves from its reference position $\mathbf{p}$ to the current position $\mathbf{x}$ at time t. If the one-to-one mapping function $\mathbf{p}(\mathbf{x}(\mathbf{y}), t)$, which gives the reference position $\mathbf{p}$ at time $t = 0$ of a spatial point $\mathbf{x}$ at time t, is known, the brain deformation can then be completely characterized. The key to the HARP method is to utilize the relationship existing between the local phase information and the mapping function to estimate the tissue deformation.

Now let $I(\mathbf{p})$ represent the intensity of a SPAMM-tagged MRI image passing through the point $\mathbf{p}$ immediately after tagging. The tagged image can be written as a finite cosine series having a certain fundamental frequency in the following

manner,

$$I(\mathbf{p}) = \sum_{k=1}^{K} D_k(\mathbf{p}) e^{j\omega_k^T \mathbf{p}}, \tag{A2}$$

where K, D_k, and ω_k are related to the parameters of the tagging pulse sequence. Replacing $\mathbf{p}$ with $\mathbf{p}(\mathbf{x}(\mathbf{y}), t)$, we can find that Eqn. (A2) can be written in terms of spatial coordinates $\mathbf{x}$ or $\mathbf{y}$ instead of material coordinates $\mathbf{p}$ as follows

$$I(\mathbf{p}(\mathbf{x},t)) = \sum_{k=1}^{K} D_k(\mathbf{p}(\mathbf{x},t)) e^{j\omega_k^T \mathbf{p}(\mathbf{x},t)} \quad \text{or} \quad I(\mathbf{y}) = \sum_{k=1}^{K} D_k(\mathbf{y}) e^{j\omega_k^T \mathbf{p}(\mathbf{x}(\mathbf{y}),t)}. \tag{A3}$$

One can see from the above equation that the SPAMM-tagged image is the sum of K complex images, called harmonic images, each corresponding to a distinct spectral peak identified by the frequency vector ω_k. The pattern of cosines in the SPAMM-tagged image is the cause of the isolated spectral peaks in its Fourier domain, and the number and distribution of spectral peaks vary according to the specific tagging pulse sequence.

One can see from Eqn. (A3) that the kth harmonic image corresponding to the frequency vector ω_k can be written as

$$I_k(\mathbf{y}, t) = D_k(\mathbf{y}, t) e^{j\omega_k^T \mathbf{p}(\mathbf{x}(\mathbf{y}),t)}. \tag{A4}$$

where D_k is called the harmonic magnitude image, and $\omega_k^T \mathbf{p}(\mathbf{x}(\mathbf{y}), t)$ is called the HARP image and denoted by ϕ_k. The HARP image is rewritten for clarity as

$$\phi_k(\mathbf{y}, t) = \omega_k^T \mathbf{p}(\mathbf{x}(\mathbf{y}), t). \tag{A5}$$

The kth harmonic image can be approximately determined by taking inverse Fourier transform of the spectral peak in the direction of ω_k, which is isolated using a band-pass filter. The magnitude image contains geometry information of the tissue without the presence of tag pattern; therefore, it is used to provide a crude segmentation that distinguishes tissue from the background for the HARP image. One can see from Eqn. (A5) that the HARP image ϕ_k is linearly related to the mapping function $\mathbf{p}(\mathbf{x}(\mathbf{y}), t)$, so it can be used to characterize the tissue motion. In actual implementation, the principal values of ϕ_k, denoted by a_k, are used since they are easily calculated from the harmonic images. Here, a_k is called the HARP angle image, and it is restricted to the range $[\pi, -\pi)$. The HARP angle image a_k is related to the HARP image ϕ_k by

$$a_k(\mathbf{y}, t) = w(\phi_k(\mathbf{y}), t), \tag{A6}$$

where the nonlinear wrapping function is given by

$$w(\phi) = \mathrm{mod}(\phi + \pi, 2\pi) - \pi. \tag{A7}$$

The displacement is defined by the difference between the current position and the original position $\mathbf{x}$, and expressed by

$$\mathbf{u}(\mathbf{y}, t) = \mathbf{x} - \mathbf{p}(\mathbf{x}, t). \tag{A8}$$

The HARP angle image can be used to obtain displacement fields of the tissue motion. Given a sequence of HARP angle images $a_k(\mathbf{y}, t)$, the following quantity can be calculated

$$\Delta a_k(\mathbf{y}, t) = w[\omega_k^T \mathbf{x}(\mathbf{y}) - \phi_k(\mathbf{y}, t)]. \tag{A9}$$

Substituting Eqns. (A5) and (A8) in to the above, we obtain

$$\Delta a_k(\mathbf{y},t) = w[\omega_k^T \mathbf{u}(\mathbf{x}(\mathbf{y}),t)]. \tag{A10}$$

Only when $\omega_k^T \mathbf{u}(\mathbf{x}(\mathbf{y}),t) \in [\pi,-\pi)$, will no wrapping occur and $\Delta a_k(\mathbf{y},t) = \omega_k^T \mathbf{u}(\mathbf{x}(\mathbf{y}),t)$. This is the only case discussed in [14]. Here we consider the more general case when $\omega_k^T \mathbf{u}(\mathbf{x}(\mathbf{y}),t)$ is not restricted to the range $[\pi,-\pi)$. For this case phase unwrapping of $\Delta a_k(\mathbf{y},t)$ is necessary to extract the displacement from equation (A10), leading to

$$w[\Delta a_k(\mathbf{y},t) + \pi] = \omega_k^T \mathbf{u}(\mathbf{x}(\mathbf{y}),t). \tag{A11}$$

Next, let $\mathbf{u}_2(\mathbf{y},t) = [u_1, u_2]$ represent the 2-D displacement within the image plane, so that $\mathbf{u}_2(\mathbf{y},t) = \mathbf{H}\mathbf{u}(\mathbf{y},t)$, and Eqn. (A11) can be rewritten as

$$w[\Delta a_k(\mathbf{y},t) + \pi] = \omega_k^T \mathbf{H}\mathbf{u}_2(\mathbf{y},t). \tag{A12}$$

If another sequence of angle images having a linearly independent frequency vector ω_l is also available, the 2-D displacement field is then calculated by

$$\mathbf{u}_2(\mathbf{y},t) = (\mathbf{W}^T\mathbf{H})^T \begin{bmatrix} w[\Delta a_k(\mathbf{y},t) + \pi] \\ w[\Delta a_l(\mathbf{y},t) + \pi] \end{bmatrix}, \tag{A13}$$

where $\mathbf{W} = [\omega_k, \omega_l]$. Equation (A13) is the key equation to calculate the 2-D displacements from the HARP angle image.

The specific slice prescription and tagging orientation in our MRI acquisition lead to the following $\mathbf{W}$ and $\mathbf{H}$ matrices for axial slice and sagittal slices, respectively.

$$\text{axial slice:} \quad \mathbf{H} = \begin{bmatrix} 1 & 0 \\ 0 & 1 \\ 0 & 0 \end{bmatrix}, \quad \mathbf{W} = \frac{2\pi}{S_p} \begin{bmatrix} 0 & 1 \\ 1 & 0 \\ 0 & 0 \end{bmatrix} \tag{A14}$$

$$\text{saggital slice:} \quad \mathbf{H} = \begin{bmatrix} 0 & 0 \\ 1 & 0 \\ 0 & 1 \end{bmatrix}, \quad \mathbf{W} = \frac{2\pi}{S_p} \begin{bmatrix} 0 & 0 \\ 1 & 0 \\ 0 & 1 \end{bmatrix} \tag{A14}$$

where $S_p = 4mm$ is the tagging period.

Department of Mechanical Science and Engineering, University of Illinois at Urbana - Champaign, Urbana, IL 61822, U.S.A.

Department of Bioengineering and Beckman Institute, University of Illinois at Urbana - Champaign, Urbana, IL 61822, U.S.A.

Department of Bioengineering and Beckman Institute, University of Illinois at Urbana - Champaign, Urbana, IL 61822, U.S.A.

School of Kinesiology, University of Michigan, Ann Arbor, MI 48109, U.S.A.

Department of Mechanical Science and Engineering, and Institute for Condensed Matter Theory and Beckman Institute, University of Illinois at Urbana - Champaign, Urbana, IL 61801, U.S.A.

E-mail: martinos@illinois.edu